Science of the Total Environment 941 (2024) 173409

Contents lists available at ScienceDirect

Science of the Total Environment

journal homepage: www.elsevier.com/locate/scitotenv

Type of probability distribution reflects how close mixing dynamics in river chemistry are to thermodynamic equilibrium

Axel Kleidon [a,1], Caterina Gozzi [b,*,1], Antonella Buccianti [b,1], Roberta Sauro Graziano [b,1]

[a] Max Planck Institute for Biogeochemistry, Jena, Germany
[b] University of Florence, Department of Earth Sciences, Firenze, Italy

HIGHLIGHTS

- Thermodynamic states are closely linked to frequency distributions.
- Type of distribution is linked to the dissipative weathering and mixing dynamics.
- Hypothesis is tested that power-law distributions are found far-from-equilibrium.
- Observations of the Arno river chemistry in central Italy confirm hypothesis.
- The extent of disequilibrium constrains the range of power-law scaling.

GRAPHICAL ABSTRACT

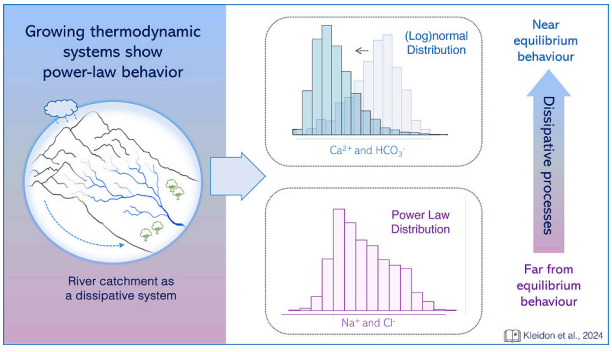

ARTICLE INFO

Editor: JV Cruz

Keywords:
Dissipation
Far from equilibrium systems
Power-law scaling
Continental weathering
Riverine chemistry

ABSTRACT

The distribution of geochemical species are typically either (log)normally distributed or follow power laws. Here we link these types of distributions to the dynamics of the system that generates these distributions, showing that power laws can emerge in dissipative systems far from equilibrium while (log)normal distributions are found for species for which the concentrations are close to equilibrium. We use observations of the chemical composition of river water from the sampling space in central Italy as well as discharge data to test this interpretation. We estimate the dissipation rate that results when groundwater drains into the river and the dissolved chemical species mix with the river water. We show that calcium (Ca^{2+}) and bicarbonate (HCO_3^-) concentrations are close to saturation along most of the downstream length of the Arno river, with decreasing dissipation rates and a lognormal distribution, while sodium (Na^+) and chloride (Cl^-) concentrations increase substantially downstream, show increased dissipation rates, and are power-law distributed. This supports our hypothesis that power law distributions appear to be indicative of dissipative systems far from thermodynamic equilibrium, while (log) normal distributions indicate weakly dissipative systems close to equilibrium. What this implies is that probability distributions are likely to be indicative of the thermodynamics of the system and the magnitude of disequilibrium constrains the range over which power-law scaling may be observed. This should help us to better

* Corresponding author.
E-mail address: caterina.gozzi@unifi.it (C. Gozzi).
[1] A.K., C.G., A.B., and R.S.G. contributed equally to this work.

https://doi.org/10.1016/j.scitotenv.2024.173409
Received 26 January 2024; Received in revised form 10 May 2024; Accepted 19 May 2024
Available online 27 May 2024

identify the generalities and mechanisms that result in these common types of distributions and to better classify variability in systems according to how dissipative these are.

1. Introduction

Geochemical elements typically show characteristic frequency distributions, being either normally or log-normally distributed (Allégre and Lewin, 1995; Limpert et al., 2001; Ott, 1990; Vistelius, 1960; Ahrens, 1954; Mitzenmacher, 2004; Aitchison and Brown, 1957; Buccianti et al., 2018), or they show a power-law distribution (van Rooij et al., 2013; Gozzi et al., 2018). A substantial body of literature aims to relate these types of distributions to the underlying processes that cause these distributions. Examples include mixing phenomena (Allégre and Lewin, 1995), repeated dilution or concentration processes (Kapteyn, 1903; Gibrat, 1930; Ott, 1990), self-organized criticality for power law distributions (Bak et al., 1987; Newman, 2005; Mitzenmacher, 2004; van Rooij et al., 2013), although power-law distributions can also emerge when frequency distributions are being combined (Porporato and Yin, 2022; Perri and Porporato, 2022).

Nevertheless, in many cases of natural systems, power-law distributions are associated with scale-invariance and are typical examples of fractal dynamics, where heavy tails represent large magnitudes of rare events and where the scaling exponent quantifies the rate of decay of the tail of the distribution. The characteristics of a fractal distribution has been suggested to be associated with mechanisms able to dissipate energy optimally and produce entropy at maximum rates (Dewar, 2003; Seely and Macklem, 2012). Other studies (Buccianti and Zuo, 2016; Buccianti et al., 2018; Kirchner and Neal, 2013) connected fractal distribution to the presence of complex irregular systems, characterized by intermittent behavior in space or time, across a range of systems (Seely and Macklem, 2012; Seely et al., 2014; Rodríguez-Iturbe and Rinaldo, 2001; Coulthard and Van De Wiel, 2007; Aguirre et al., 2009; van Rooij et al., 2013; Sornette, 2006). The use of multifractals in the applied sciences has been correlated with the presence of multiplicative cascade events and the necessity to describe phenomena with an entire spectrum of generalized fractal dimensions. In this case, sparser and denser regions of a time/space distribution might have different scaling behaviors (Mandelbrot, 2003; Dentz et al., 2023).

Here, we focus on a case in which power laws emerge in a natural dissipative system. This link between the dissipative behavior of a process and the frequency distribution of the involved variables is yet unclear. We aim to link these distributions to the thermodynamic setting in which these are generated, particularly how these are linked to the dissipative dynamics associated with the depletion of disequilibrium conditions within the Earth system (Kleidon, 2012, 2016). Note that we use the terms disequilibrium and equilibrium strictly with reference to the thermodynamic state, i.e., in reference to states of maximum entropy, and not in reference to whether a system has reached a steady state, i.e., that the mean of a variable does not change in space or time. A steady state may indicate that a system exhibits no dynamics, either because it has reached thermodynamic equilibrium or because of other constraints that prevent dynamics to occur, e.g., for very slow kinetics of the chemical reactions involved. Both cases are non-dissipative systems, while here we focus on dissipative systems that actively deplete their state of disequilibrium. We hypothesize that power laws are found in such dissipative systems in far-from-equilibrium conditions. Power law distributions can then be seen as an indication for a special type of dissipative, thermodynamic systems. This, in turn, should have wider-ranging implications in that this insight should hold for many environmental variables that are associated with thermodynamic Earth system processes. Such a thermodynamic link may then supplement previous explanations - after all, the suggested mechanisms such as mixing phenomena and repeated dilution or concentration are all irreversible, dissipative processes.

To link frequency distributions with the thermodynamic behavior, we use concentrations of dissolved chemical species in river water within the Arno catchment in central Italy as our thermodynamic system (Fig. 1a). These concentrations are routinely measured over the whole catchment. The thermodynamic disequilibrium is caused when precipitation adds essentially desalinated water to the surface, which is in disequilibrium with the minerals of the regolith of the Arno catchment (Fig. 1b). Chemical weathering reactions within the critical zone deplete this disequilibrium, so that concentrations in groundwater increase. As this groundwater drains into the river, its chemical composition mixes with river water, resulting in concentrations within river water to increase (for conservative species that are not further transformed e.g., by metabolic activities within the river water). Hence, the concentrations of chemical species are expected to increase from the spring of the Arno river to its mouth, reaching concentrations closer to or at equilibrium when it drains into the sea. This, however, takes place at contrasting rates, depending on the minerals, the regolith, and the weathering reactions involved.

How, then, is the frequency distribution of concentrations reflective of the thermodynamics of the system? A substance containing a species that weathers fast, like calcium, reaches saturated concentrations and thus a state of thermodynamic equilibrium relatively quickly. This trend towards saturation, including a certain degree of random variations, is illustrated using artificial data in Fig. 1c. Saturation represents our reference state of thermodynamic equilibrium here because it is at this state at which the rates of dissolution of minerals and their precipitation into the solid state balance each other. This is a consequence of the Law of Mass Action and equivalent to chemical equilibrium, in which the rates of the forward (dissolution) and backward (precipitation) chemical reactions are equal.

This equilibrium state is then perturbed by random variations in the input to the river. Input from supersaturated groundwater, from unsaturated surface runoff after a rainfall event, or discharge of sub-basins represent sources of variability to the input of water and weathered material into the river. Note, however, that these random variations are macroscopic in their nature, that is, expressed in variations in thermodynamic variables which assume local thermodynamic equilibrium, and not related to fluctuations at the microscopic, molecular scale in statistical mechanics. The resulting chemical disequilibrium in the river water – characterized by macroscopic, thermodynamic variables – is then depleted once mixed within the river. Because these random variations can perturb the equilibrium state more or less equally in both directions, we would expect a symmetric distribution of the composition.

This thermodynamic setting of such a weakly dissipative system near equilibrium should then be linked to a (log)normal distribution (Fig. 1c), depending on the prevalence of additive or multiplicative phenomena (van Rooij et al., 2013). When perturbations add water and dissolved material, thus representing a multiplicative mixing, this case has previously been linked to a lognormal distribution (Allégre and Lewin, 1995). In either case, this mixing is associated with dissipation, although the levels should be relatively small and continuous along the course of the river because it is already close to or at thermodynamic equilibrium. A lognormal distribution is thus likely to represent a system that is near equilibrium, where the effect of trends within the system is small. Because the perturbations of thermodynamic equilibrium are relatively small, this weakly dissipative system should also have little autocorrelation in its spatiotemporal variability.

When we then look at those minerals that are weathered strongly, but their concentrations do not reach equilibrium but remain far from equilibrium because the disequilibrium is very large, we should expect

power-law scaling across scales (Mandelbrot, 2003; Dentz et al., 2023). To explain this, we use the interpretation of power laws in economics (Gabaix, 2016), where it has been shown that power laws are the outcome of proportionate random growth in the presence of weak friction. In this explanation, the growth of each entity in the system (Gabaix considered firms in an economy, Gabaix (2016)) is proportional to its size (with random variations), which results in exponential growth. Yet, the presence of friction causes some of the entities to drop out, ensuring overall a steady-state of the system.

Applied to our river catchment, we do not have proportionate random growth, but for some minerals a proportionate random increase of the weathering rates along the main branch of the river. The rate of weathering is proportional to the magnitude of disequilibrium, leading to an exponential depletion of this disequilibrium. This is superimposed by the same variability as above, that is, by random input perturbations of groundwater, sub-basins, and surface runoff. When the initial disequilibrium is large and the depletion rate is small compared to the disequilibrium, then the state of saturation is not reached within the catchment. The "friction" of Gabaix's interpretation is then the slow depletion of the disequilibrium state. The power-law distribution should thus be reflective of a far-from-equilibrium system with a trend towards equilibrium. This trend is illustrated with artificial data in Fig. 1d. Because of the trend, we should find that the autocorrelation within the system is greater than the near-equilibrium system described above.

We test these interpretations with the observations from the Arno catchment. For the thermodynamic interpretation, we developed a simple model described in the next section and combined it with these observations to capture the mean trends and to infer the level of dissipation associated with different chemical species and their distributions.

2. Materials and methods

To link probability distributions with the thermodynamics of the system, we considered the concentrations of major elements in river water within the Arno river basin in central Italy. These concentrations were combined with discharge data and interpolated with Hack's law to diagnose the intensity of dissipation by river mixing.

2.1. Observations of river concentrations and discharge

The Arno river is the most important basin in the Tuscany Region and the fifth largest in Italy with a catchment surface area of 8228 km^2 and a course of 242 km. The river springs out from Mt. Falterona (1654 m a.s.l.), in the Northern Apennines, and flows towards south-west up to the mouth, faced to the Ligurian Sea and placed in the coastal area of the city of Pisa (Fig. 1a).

The annual rainfall pattern is typical of the Mediterranean region, with a low regime in summer (minimum in August) and two peaks of precipitation in winter (December and February–March). Since the majority of the basin is characterized by low-permeability rocks, an efficient infiltration under the surface is hindered, thus facilitating surface runoff. With a slight delay, discharge variations follow those of precipitation events (Dinelli et al., 2005). This particularly applies to mountain regions, where strong and abrupt flow regime variations can occur, also because of the scarce presence of permanent springs. Mean annual rainfall ranges from 600 mm in the lowlands up to 3000 mm on the Apennine ridge (Nisi et al., 2008). Higher discharge pertain to the Chiana and Sieve rivers and the wider gaps between rainfall and discharge take place in Chiana, Sieve and Elsa sub-basins. Areas with lower differences in rainfall and discharge are those characterized by higher elevation and lower temperature, with more surface runoff and

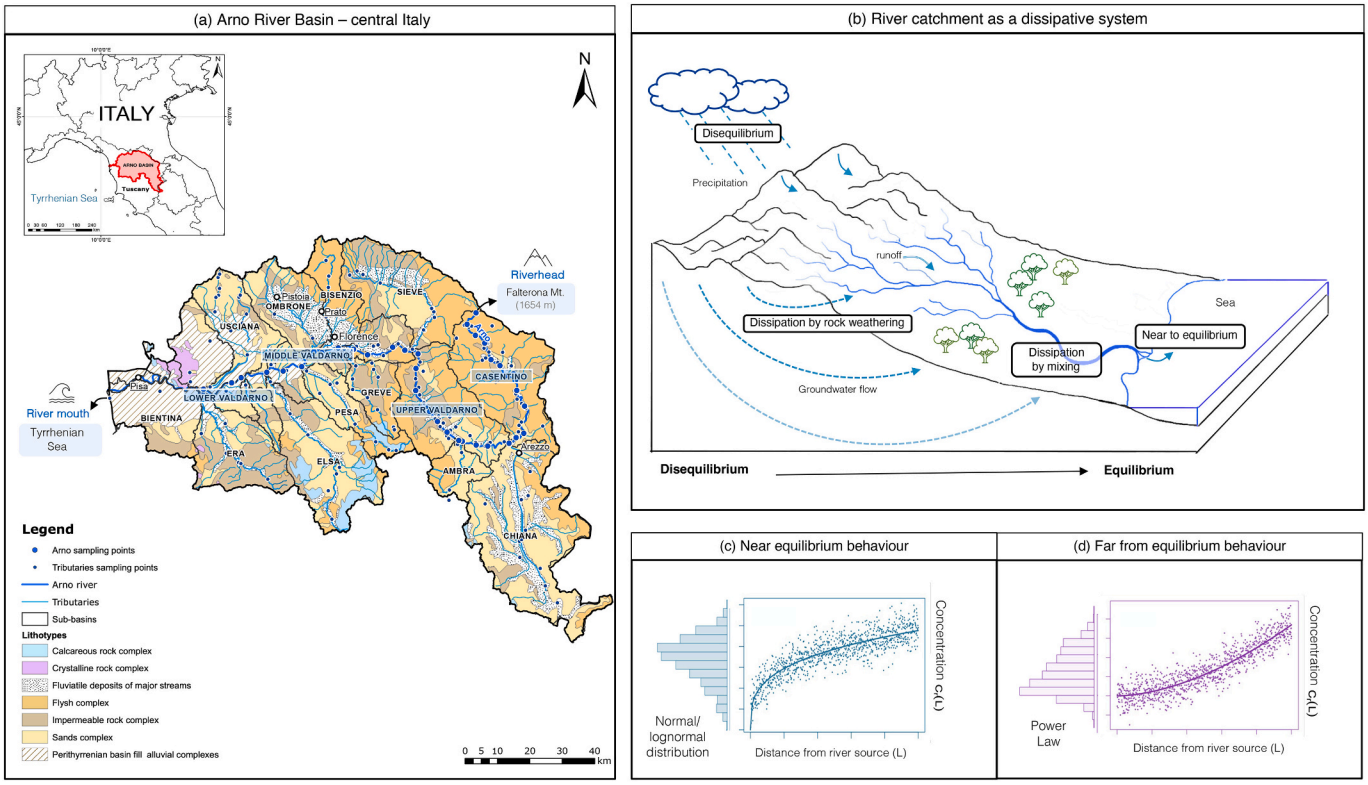

Fig. 1. (a) Geological map of the Arno river basin in central Italy including its sub-basins and sampling points; (b)weathering in a river catchment as a dissipative, thermodynamic system; (c) near equilibrium behavior and (log)normal distribution; (d) far from equilibrium behavior and power law distribution. Examples (c) and (d) are based on hypothetical data for illustration.

lower evapotranspiration (Nisi, 2005a). For what concerns the outcropping rocks, the Arno river basin is featured mainly by the presence of sedimentary folded and faulted Mesozoic and Tertiary units (Abbate et al., 1992; Moretti, 1994), related to the Apennine orogeny (Elter et al., 1975; Boccaletti and Coli, 1983; Carmignani et al., 1994; Cortecci et al., 2002).

We used a subset of species from the chemical composition of 508 samples (473 riverine cases, 31 springs) of Ca^{2+}, Mg^{2+}, Na^{+}, K^{+}, HCO_3^-, CO_3^{2-}, SO_4^{2-}, Cl^-, SiO_2, F^-, Br^-, B, NH_4^+, NO_2^-, and NO_3^-. Details of the analytical methodologies can be found in Nisi (2005b). The samples were collected in different periods to take into account seasonal variations, changes in the flow regime and more long time-scale effects.

2.2. Diagnosing dissipation by river water mixing

We estimated the dissipation, D_{mix}, associated with mixing the chemical species of river water with the water input using the observations as well as mass balances for river water and chemical species. We use the downstream distance, L, of the main branch of the Arno river from its source as our independent variable. The main variables to quantify dissipation are then the river discharge, Q, and the concentrations c of dissolved minerals in the river water, c_r, and in the groundwater, c_g. We assume that the main, climatological variation in these variables is along the downstream distance L and do not treat their temporal variations. Note also that these variables have inherently random contributions, as discussed in the introduction. Here, we neglect this random component and focus only on the mean variation of these variables along the downstream distance L. The observations of discharge and measured concentrations are then used together with the analytic descriptions derived below to estimate the dissipation rates by mixing along the river.

We used the observations of discharge from the Arno basin and fitted these to Hack's law (Hack, 1957) to get an explicit relationship of how river discharge, Q (in units of litres/second, L/s), along the main branch varies with distance, L, from the source. Hack's law is commonly written as

$$L = \gamma \cdot Q^{\alpha} \tag{1}$$

where γ is a conversion factor and $\alpha \approx 0.59$ is the Hack's exponent, which can be explained by the fractal scaling of river basins (Rinaldo et al., 1992). We can also reformulate Hack's law to make the downstream distance our main, independent variable and express discharge as a function of L. This yields:

$$Q = \left(\frac{L}{\gamma}\right)^{1/\alpha} \tag{2}$$

with an exponent of $1/\alpha \approx 1.69$, and a value of $\gamma = (L/Q^{\alpha}) \approx 0.41$ for the Arno river basin with L in km and Q in L/s.

In the fitting of concentrations to observations, we distinguished two cases: In Case A the concentrations are close to saturation and thermodynamic equilibrium (i.e., $c_r \approx c_{sat}$), while in Case B, the initial stage is far from equilibrium (i.e., $c_r \ll c_{sat}$). Case A was then fitted to a power law of the form

$$c_r(L) \approx a \cdot L^b. \tag{3}$$

For Ca^{2+}, we obtain a best fit with values of $a = 2.73 \cdot 10^{-4}$ and $b = 0.356$ with a $r^2 = 0.43$ and RMSE $= 7.69$, while for HCO_3^-, we obtained $a = 1.48 \cdot 10^{-3}$ and $b = 0.172$ with a $r^2 = 0.80$ and RMSE $= 0.07$ mol/L.

In case B, the concentrations are far from saturation (i.e., far from thermodynamic equilibrium), and follow approximately an exponential growth

$$c_r(L) \approx a \cdot e^{bL}. \tag{4}$$

For Na^{+}, we obtain a best fit with values of $a = 2.08 \cdot 10^{-4}$ and $b = 0.018$ with a $r^2 = 0.93$ and RMSE $= 0.12$, while for Cl^-, we obtained $a = 1.59 \cdot 10^{-4}$ and $b = 0.017$ with a $r^2 = 0.94$ and RMSE $= 0.12$ mol/L.

We next infer the concentrations, c_g, of the chemical compounds in the water that is added to the river by the mass balance of the chemical compound within river water,

$$\frac{d(c_r Q)}{dL} = c_r \cdot \frac{dQ}{dL} + \frac{dc_r}{dL} \cdot Q = c_g \cdot \frac{dQ}{dL}. \tag{5}$$

Note that this formulation of the mass balance only considers the mean variations along the downstream distance L and neglects the role of random variations.

Using Hack's law (Eq. 2), this can be used to infer the concentrations c_g:

$$c_g = c_r + \alpha L \cdot \frac{dc_r}{dL} \tag{6}$$

where the term dc_r/dL is calculated from Eq. 3 or 4 with the respective parameters for the chemical species.

The dissipation due to the mixing of chemical compounds of the added water with river water is then calculated using chemical potentials, $\mu = \mu_0 + RTlnc$, where μ_0 is a reference chemical potential, R is the molar gas constant, and T is temperature. Dissipation, D_{mix}, is then given by

$$D_{mix} = -\frac{d(c_r \cdot Q \cdot \mu_r)}{dL} + c_g \cdot \frac{dQ}{dL} \cdot \mu_g. \tag{7}$$

Using the mass balance (Eq. 5), this expression can be rearranged into

$$D_{mix} = -\frac{RT}{Q} \cdot \left((c_g - c_r) + c_g \cdot ln(c_r/c_g) \right) \cdot \frac{dQ}{dL} \tag{8}$$

where c_g is calculated from Eq. 6, c_r from Eq. 3 or 4, and dQ/dL from Eq. 2 using the fitted parameters as well as the values of γ and α to calculate Q.

We calculate D_{mix} as follows: river discharge $Q(L)$ is described by Eq. 2, with parameter values $\alpha = 0.59$ and $\gamma = 0.41$ for the Arno river basin. The concentration of river water $c_r(L)$ is obtained for each chemical species from Eq. 3 or 4. The concentration of added water $c_g(L)$ is then inferred from Eq. 6. With the functions Q, c_r, and c_g being specified, we can then use Eq. 8 to calculate the dissipation rate D_{mix}.

2.3. Power-law fitting

We used the PLFIT(x) function of Matlab to estimate x_{min} and the scaling exponent k according to the goodness-of-fit-based method described in Clauset et al. (2009). The function uses a vector of observations of some quantity x (our river concentrations $c_r(L)$) to which we wish to fit the power-law distribution $P(x) \sim x^{-k}$ for $x \geq x_{min}$. The fitting procedure works as follows: 1) For each possible choice of x_{min}, k is estimated via the method of maximum likelihood, and the calculus of the Kolmogorov-Smirnov goodness-of-fit statistic D; and 2) the estimate of x_{min} is the value that gives the minimum value D over all values of x_{min}.

3. Results and discussion

3.1. Downstream variations of discharge, composition, and dissipation

To link the distribution of chemical species within the Arno river with their extent of disequilibrium and level of dissipation, we first consider their downstream variations along the main branch. These are shown in Fig. 2.

While measurements of chemical concentrations are directly available (Fig. 2b), to diagnose the associated dissipation due to mixing, we also need the discharge volume flux as a function of downstream

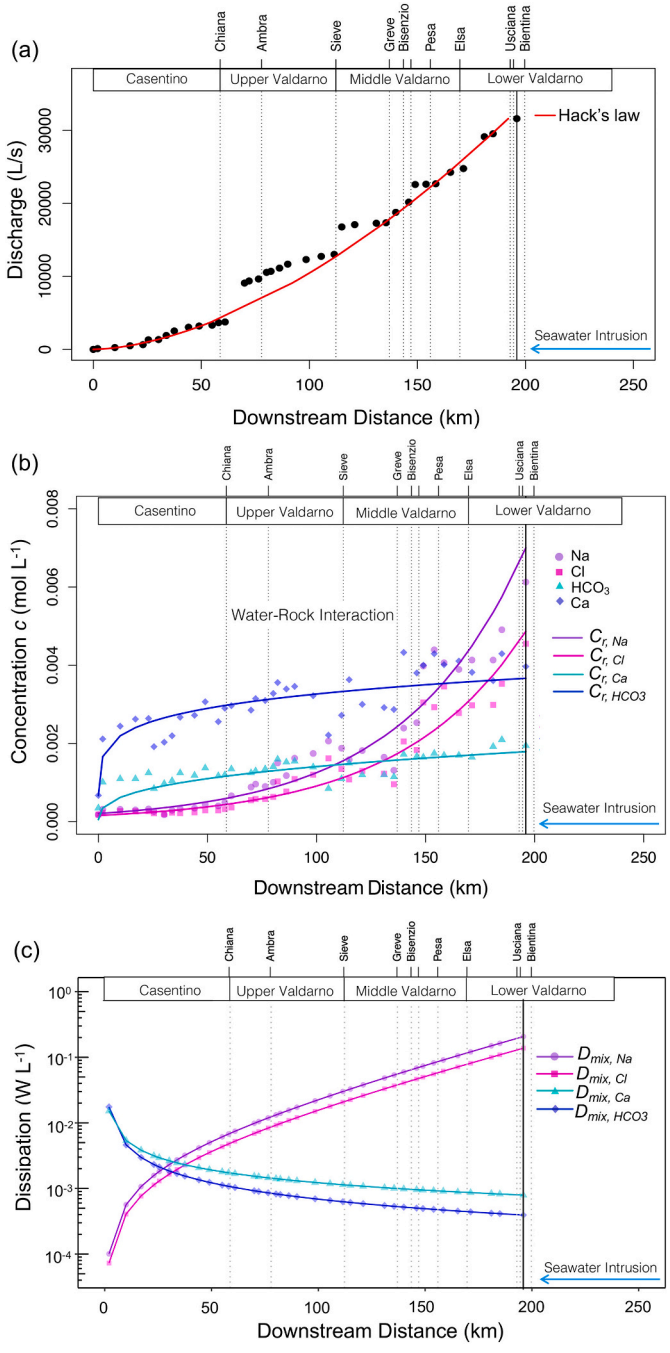

Fig. 2. (a) River discharge (Q, in units of litres per second, L/s) as a function of downstream distance (L, in units of kilometers, km) with observations marked by the black circles and the interpolation using Hack's law shown by the red line. (b) Concentrations of chemical species in river water (c_r, in units of moles per litre, mol/L), along the downstream distance, with observations marked by dots and lines representing the fitted model. (c) Dissipation by mixing of groundwater with river water (D_{mix}, in units of Watt per litre, W/L) for the four chemical species considered, normalized by discharge.

distance (Fig. 2a). We used observations of discharge and fitted Hack's law to these to get a functional relationship of river discharge Q as a function of downstream distance L (red line in Fig. 2a). We obtained a relationship $Q(L) = 0.416 \cdot L^{1.69}$, with L in units of km, Q in units of litres per second, L/s, 0.416 is a parameter obtained from fitting, and 1.69 is the inverse of the typical value for the Hack exponent of 0.59 (Rinaldo et al., 1992).

To have functional relationships for the mean variation of chemical concentrations along the river, we distinguished two cases: Case A represents chemical species close to equilibrium for which we expect a (log)normal distribution. Their concentrations were fitted to a power law of the form $c_r(L) \propto a \cdot L^b$. Case B assumes the species being far from equilibrium, for which we expect power-law scaling. Their concentrations were fitted to an exponential function, $c_r \propto a \cdot e^{bL}$. The fits are shown by the solid lines in Fig. 2b. The parameters obtained for the fit as well as the r^2 values for the four chemical species considered are provided in the Material and Methods section.

To estimate the dissipation by mixing, we need the increase of river flow as well as the increase in concentration. From the derivatives dQ/dL and dc_r/dL we obtain the addition of streamflow as well as dissolved species as a function of L, from which we can then calculate the rate of dissipation, D_{mix}, due to the addition of water and dissolved species to the river (Eq. 8).

The resulting trends are shown in Fig. 2c. We note that the concentrations of calcium (Ca^{2+}) and bicarbonates (HCO_3^-) quickly saturate along the main branch and only increase slightly with downstream distance. The concentrations of sodium (Na^+) and chloride (Cl^-), however, increase nearly exponentially with downstream distance. This results in different variation in the dissipation: while calcium and carbonates show low levels of dissipation with river water, the dissipation of mixing increases substantially for sodium and chloride with downstream distance.

3.2. Linking distributions with dissipative behavior

We next link the diagnosed values of dissipation back to the distribution of chemical species. To do so, we used the observed concentrations of Ca^{2+}, HCO_3^-, Na^+, and Cl^- within the whole Arno catchment and sorted them by abundance to infer their complementary cumulative distribution function (CCDF). The CCDF is defined as the cumulative probability Pr of concentrations C_r exceeding c_r, i.e. $Pr[C_r \geq c_r]$. A power law distribution is then identified in a log-log plot against the logarithm of the concentration ($ln(c_r)$) when the CCDF follows a straight line. This provides a simple empirical test for whether a variable follows a power-law distribution (Mitzenmacher, 2004).

In Fig. 3, we show the CCDFs as well as what would be expected for a lognormal distribution, obtained from the mean and variance derived from observed data (colored lines). The lognormal distribution describes the behavior of Ca^{2+} and HCO_3^- very well (Fig. 3b, Kolmogorov-Smirnov test with $p > 0.05$, null hypothesis H_0 of lognormality accepted). For Na^+ and Cl^-, there are marked deviations from lognormal scaling ($p < 0.05$, null hypothesis H_0 of lognormality refused), and a power-law fit yields a better description above a certain threshold concentration (Fig. 3b).

To identify this threshold and obtain a power-law fit, we used the approach of Clauset et al. (2009) and calculated the likelihood estimators for fitting the power-law distribution of the form $p(c_r) \propto c_r^{-k}$ for concentrations above a threshold $c_r \geq c_{r,min}$ to the data of Na^+ and Cl^- (see Materials and methods section). The scaling parameter k (i.e., the slope in the log-log plot) and the value for the threshold $c_{r,min}$ were estimated, associated with the minimum value of the Kolmogorov-Smirnov goodness-of-fit statistic. For Na^+ a power law behavior was obtained for $c_r \geq 0.0022$ mol/L (51.2 mg/L) ($k = 3$), and for Cl^- for $c_r \geq 0.0021$ mol/L (72.7 mg/L) ($k = 3.2$). The logarithms of the obtained estimations for $c_{r,min}$ in mol/L are shown in Fig. 3a and c as vertical lines and correspond to $ln(c_r) = -6.11$ and -6.19 for Na^+ and Cl^-, respectively.

Fig. 3c and d shows the associated rates of dissipation by mixing. By comparison we note that the onset of the power-law scaling behavior for Na^+ and Cl^- corresponds to a change in dissipative behavior, where it reflects a steady increase using the log-scale, i.e., the dissipation by mixing also increases exponentially. The onset of power-law scaling thus

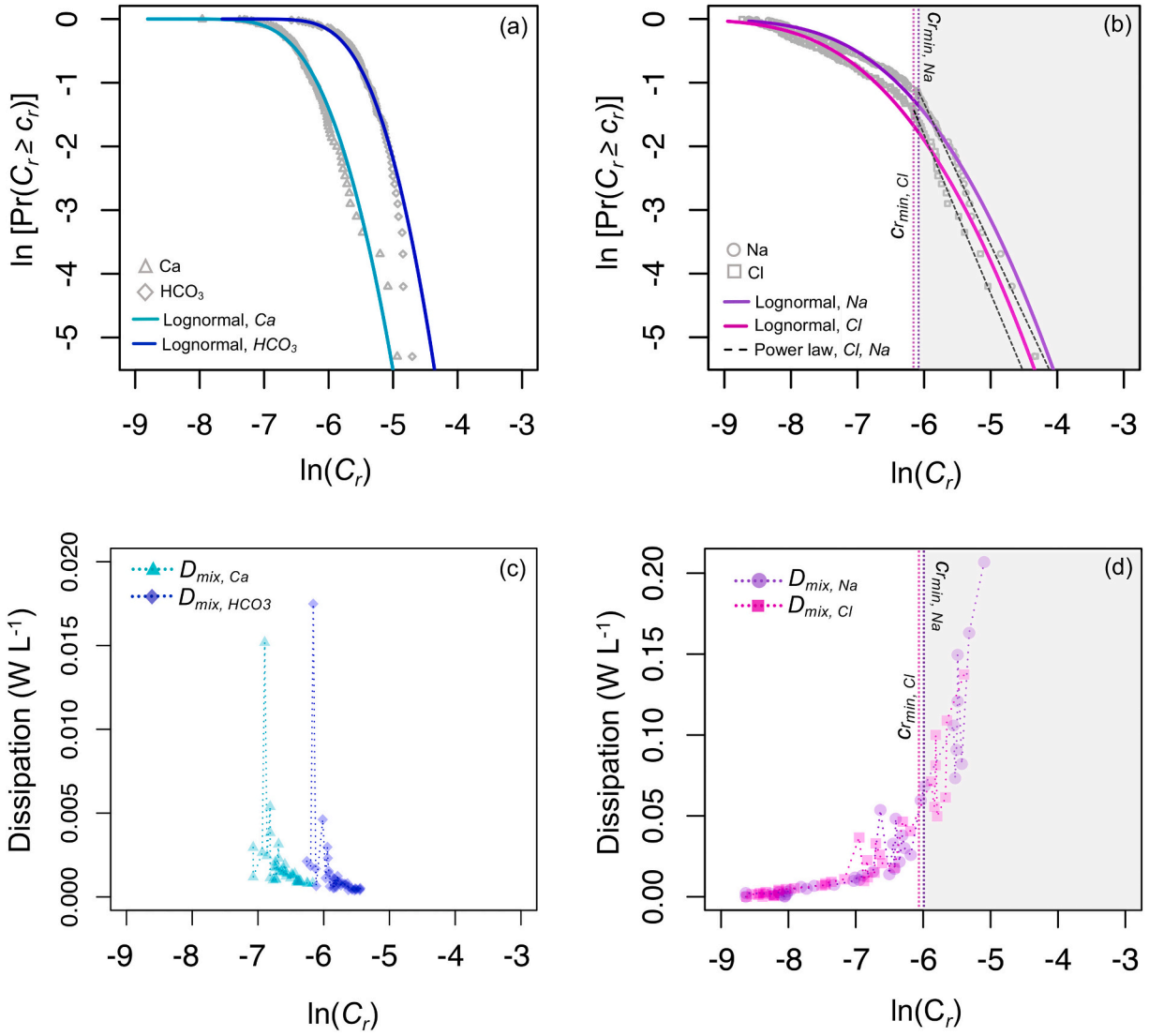

Fig. 3. Complementary cumulative distribution function CCDF for the natural logarithm of the concentrations ($ln(c_r)$) of (a) Na^+, Cl^- and (b) Ca^{2+}, HCO_3^-. The colored curves reflect a fit to a lognormal distribution obtained from the obtained with mean and variance of observed data, the black dashed line represents a power law distribution. (c) and (d) show the associated, diagnosed values of dissipation by river mixing (D_{mix}, in units of Watt per litre, W/L). The vertical lines in (b) and (d) indicate thresholds ($c_r > c_{r,min}$) above which a power-law scaling yields a more adequate fit (Kolmogorov-Smirnov goodness-of-fit statistics).

appears directly related to the increased dissipation for Na^+ and Cl^- in the regime where their concentrations show an exponential-like growth of concentrations of Na^+ and Cl^- with downstream distance. For Ca^{2+} and HCO_3^- we see a substantially different pattern in dissipation, which is rapidly declining with downstream distance and exhibits very low magnitudes compared to Na^+ and Cl^-. The dissipative behavior of mixing thus appears to be indicative of the onset and presence of power-law scaling.

3.3. Dissipation and compositional data

To test whether the obtained relationships are due to the composition of river water rather than that of single species, we applied compositional analysis to the data (Aitchison, 1982; Gozzi and Buccianti, 2022; Buccianti and Gozzi, 2021). The subcomposition given by Ca^{2+} and HCO_3^-, and Na^+ and Cl^- is transformed according to Egozcue et al. (2003); Gozzi et al. (2020) to obtain independent real coordinates. The values of the isometric log-ratio between HCO_3^- and Ca^{2+} versus Cl^- and Na^+ are analyzed as a function of the D_{mix} values of Cl^- and Na^+. The isometric log-ratio values are obtained by applying the partition method as reported in Egozcue et al. (2003). As shown in Fig. 4, the dissipation is a feature of the sub-composition that is maintained even when the relationships among all the variables are taken into account. The dissipation due to mixing processes is a property of the composition and not only of single species.

3.4. Interpretation and implications

The chemical species we considered in our analysis are relatively conservative — their concentration is not altered much by, e.g., biotic activity within the river (which alters silicates) or by agriculture (with inputs of nitrate and potassium). Hence, we obtain a relatively clear scaling behavior and distribution function as a function of downstream distance. This specific application may thus not necessarily be applicable to other, non-conservative species. Nevertheless, the scaling behavior we found results from the dissipation of the mixing process. That is, it is a property of the composition, and not only of a single species. This is confirmed by compositional analysis that separates the composition of river water into independent variables (Aitchison (1982); Egozcue et al. (2003); Gozzi et al. (2020), see Section 3.3.). Also,

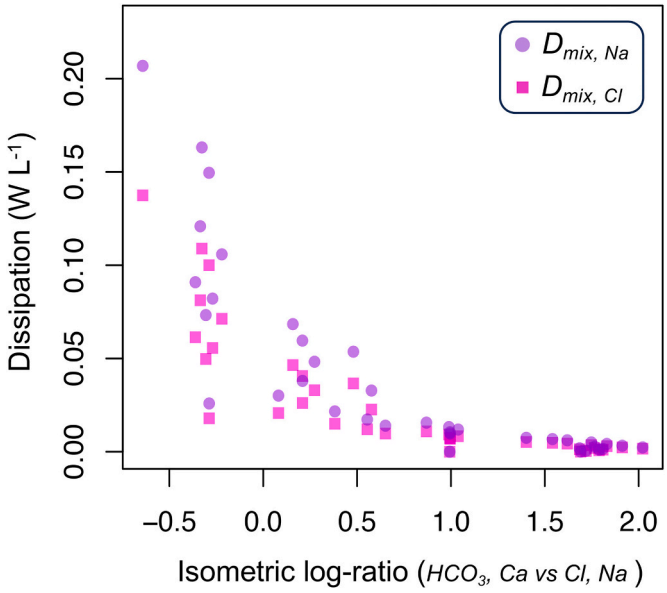

Fig. 4. Isometric log-ratio between HCO_3^- and Ca^{2+} versus Cl^- and Na^+ represented as a function of the dissipation by river mixing (D_{mix}, in units of Watt per litre, W/L) for the values of Cl^- and Na^+.

we did not account for variations in the regolith or specifics of the reaction kinetics. These factors may limit the general insights we can gain for weathering dynamics to some extent.

The analysis with respect to dissipation nevertheless provides some insights on how weathering dynamics are related to the dissipation of mixing. In the case of Ca^{2+} and HCO_3^-, the concentrations are governed by both the availability of elements and solubility reactions related to fast kinetics. In the case of Na^+ and Cl^-, the lower availability and the lack of common solubility reactions restrict their weathering reactions. Thus, it is possible to conclude that for Ca^{2+} and HCO_3^-, dissipation takes place almost entirely by weathering within the critical zone, so dissipation within the river is low, while for Na^+ and Cl^-, more of this dissipation takes place when the added water mixes with river water. In other words, the change in dissipation along the downstream distance is indicative of the intensity of weathering dynamics in the critical zone.

We can also derive more general insights from our analysis, linking these back to the general question of how the distribution of geochemical species is related to dissipative dynamics, and, more generally, to the link between power-law scaling and thermodynamic systems.

Our analysis links closely to the interpretation of power-law behavior of Gabaix (Gabaix, 2016). For Na^+ and Cl^-, we observe a large disequilibrium in concentrations, an exponential increase in mean concentration (Fig. 2b) and dissipative behavior along downstream distance (Fig. 2c). This directly relates to the proportionate growth in Gabaix's explanation for power-law emergence (Gabaix, 2016). Hence, we find this scaling for these chemical species (Fig. 3d). In the absence of this exponential growth, as in our cases of Ca^{2+} and HCO_3^-, the concentrations do not increase much (Fig. 2b) and the magnitude of dissipation (Fig. 2c) decreases along the river. Consequently, the resulting concentrations are shaped by (log)normal scaling behavior (Fig. 3c).

Our interpretation is consistent with an alternative interpretation of how power laws emerge from history-dependent processes that reduce the sample space due to their breaking of symmetry (Corominas-Murtra et al., 2018). The connection to our thermodynamic interpretation is that the history – or memory, or the sample space – of the system reflects the disequilibrium state, while the breaking of symmetry relates to the preferential direction towards thermodynamic equilibrium. The reduction of the sample space then is represented by the dissipation of the disequilibrium state. While not all cases of power laws are thermodynamic processes, when it comes to environmental processes, these are generally thermodynamic in their nature and typically related to disequilibrium states.

What our thermodynamic interpretation adds to these explanations is that the dynamics are related to the presence of thermodynamic disequilibrium within the system. A disequilibrium state is non-trivial, as it typically requires a system to perform work to maintain such disequilibrium states within the Earth system (Kleidon, 2012) and this work is thermodynamically limited as well (Kleidon, 2023). The degree of disequilibrium then sets an upper bound to the range over which power-law scaling may be observed. Furthermore, the depletion of disequilibrium is typically what drives dynamics, so that the magnitude of processes are related to the degree of disequilibrium. This proportionality links, again, to Gabaix's stochastic proportionate growth as a prerequisite of finding power-law scaling. We thus gain an interpretation of power-law scaling that is embedded within the general thermodynamic setting of Earth system processes.

Our interpretation should thus be applicable to a wide range of Earth system processes that reflect power-law scaling behavior. To illustrate this wider applicability, we can consider other instances of power-law scaling of Earth system processes, e.g., forest fires (Malamud et al., 1998), clouds (Lovejoy, 1982), or earthquakes (Bak and Tang, 1989). Forest fires deplete the disequilibrium represented by reduced carbon in biomass and atmospheric oxygen, clouds deplete the disequilibrium in form of the latent heat stored in water vapor, while earthquakes dissipate the energy stored in stresses within the Earth's crust. It should thus be possible to frame power laws of these (and other) cases in the general context of thermodynamic disequilibrium despite the nature of the associated disequilibrium being rather different.

4. Conclusions

We used observed variations in chemical composition along the Arno river in Central Italy and linked the resulting frequency distributions to their respective thermodynamic state. The chemical species of Ca^{2+} and HCO_3^- weather rapidly, their river concentrations are close to saturation and thermodynamic equilibrium, and their frequency distributions follow a lognormal distribution. On the other hand, Na^+ and Cl^- react more slowly, their concentrations remain far from equilibrium, and their distributions show power-law scaling. The presence of power-law scaling in our case is thus representative of a dissipative system far

from thermodynamic equilibrium, while (log)normal distributions appear to be representative of systems close to thermodynamic equilibrium.

We showed that this thermodynamic interpretation of power-law behavior is consistent to previous explanations of proportionate random growth (Gabaix, 2016) and sample-space reduction Corominas-Murtra et al. (2018). When thermodynamic systems are far from equilibrium, the dissipation is typically proportional to the disequilibrium, thus resulting in proportionate change, as required by Gabaix's interpretation. At the same time, disequilibrium represents memory of the system, and the dissipation of disequilibrium is associated with a reduction of this memory, resulting in sample-space reduction (Corominas-Murtra et al., 2018).

What this implies is that frequency distributions in natural thermodynamic systems are indicative of the thermodynamic state of that system. Since power-law scaling is associated with disequilibrium, which needs work to be generated, this means that thermodynamics should set the range over which power-law scaling can be observed for Earth system processes, and, more generally, on the magnitude of variability. This would, however, require further investigations.

CRediT authorship contribution statement

Axel Kleidon: Writing – review & editing, Writing – original draft, Methodology, Conceptualization. **Caterina Gozzi:** Writing – review & editing, Visualization, Software, Investigation, Formal analysis. **Antonella Buccianti:** Writing – review & editing, Writing – original draft, Supervision, Resources. **Roberta Sauro Graziano:** Writing – review & editing, Software, Investigation, Formal analysis.

Declaration of competing interest

The authors declare that they have no known competing financial interests or personal relationships that could have appeared to influence the work reported in this paper.

Data availability

Data will be made available on request.

Acknowledgments

A.K. thanks the Univ. Firenze for the hospitality and a visiting professorship. Funder: Project funded under the National Recovery and Resilience Plan (NRRP), Mission 4 Component 2 Investment 1.4 — Call for tender No. 3138 of 16 December 2021, rectified by Decree no. 3175 of 18 December 2021 of Italian Ministry of University and Research funded by the European Union – NextGenerationEU.

Award Numbers: Project codes CN_00000033 and CN_00000013, Concession Decree No. 1034 of 17 June 2022 adopted by the Italian Ministry of University and Research, CUP: B83C22002910001 and B83C22002830001, Project titles "National Biodiversity Future Center — NBFC" (A.B and C.G) and "National Centre for HPC, Data and Quantum Computing" (A.B).

References

Abbate, R., Castellucci, P., Ferrini, G., Pandeli, E., 1992. I dintorni di Firenze. In: Guide Geol. Reg., vol. 4 Società Geologica Italiana, pp. 214–223.

Aguirre, J., Viana, R.L., Sanjuán, M.A.F., 2009. Fractal structures in nonlinear dynamics. Rev. Mod. Phys. 81, 333–386.

Ahrens, L.H., 1954. The lognormal distribution of the elements (2). Geochim. Cosmochim. Acta 6, 121–131.

Aitchison, J., 1982. The statistical analysis of compositional data. J. R. Stat. Soc. Ser. B Method. 44, 139–177.

Aitchison, J., Brown, J.A.C., 1957. The Lognormal Distribution. Cambridge University Press, Cambridge, UK.

Allégre, C.J., Lewin, E., 1995. Scaling laws and geochemical distributions. Earth Planet. Sci. Lett. 132, 1–13.

Bak, P., Tang, C., 1989. Earthquakes as a self-organized critical phenomenon. J. Geophys. Res. Solid Earth 94, 15635–15637. URL: https://doi.org/10.1029/JB094iB11p15635.

Bak, P., Tang, C., Wiesenfeld, K., 1987. Self-organized criticality: an explanation of the 1/f noise. Phys. Rev. Lett. 59, 381–384.

Boccaletti, M., Coli, M., 1983. La tettonica della Toscana: assetto ed evoluzione. Mem. Soc. Geol. Ital. 25, 51–62.

Buccianti, A., Gozzi, C., 2021. The whole versus the parts: The challenge of compositional data analysis (CoDA) methods for geochemistry. In: Filzmoser, P., Hron, K., Martín-Fernández, J.A., Palarea-Albaladejo, J. (Eds.), Advances in Compositional Data Analysis: Festschrift in Honour of Vera Pawlowsky-Glahn. Springer International Publishing, Cham, pp. 253–264.

Buccianti, A., Zuo, R., 2016. Weathering reactions and isometric log-ratio coordinates: do they speak to each other? Appl. Geochem. 75, 189–199.

Buccianti, A., Lima, A., Albanese, S., De Vivo, B., 2018. Measuring the change under compositional data analysis (CoDA): insight on the dynamics of geochemical systems. J. Geochem. Explor. 189, 100–108.

Carmignani, L., Decandia, F.A., Fantozzi, P.L., Lazzarotto, A., Liotta, D., Meccheri, M., 1994. Tertiary extensional tectonics in Tuscany (Northern Apennines, Italy). Tectonophysics 238, 295–315.

Clauset, A., Shalizi, C.R., Newman, M.E.J., 2009. Power-law distributions in empirical data. SIAM Rev. 51, 661–703.

Corominas-Murtra, B., Hanel, R., Zavojanni, L., Thurner, S., 2018. How driving rates determine the statistics of driven non-equilibrium systems with stationary distribution. Sci. Rep. 8, 1–9.

Cortecci, G., Dinelli, E., Bencini, A., Adorni-Braccesi, A., La Ruffa, G., 2002. Natural and anthropogenic SO_4 sources in the Arno river catchment, northern Tuscany, Italy: a chemical and isotopic reconnaissance. Appl. Geochem. 17, 79–92.

Coulthard, T.J., Van De Wiel, M.J., 2007. Quantifying fluvial non linearity and finding self organized criticality? Insights from simulations of river basin evolution. Geomorphology 91, 216–235.

Dentz, M., Kirchner, J., Zehe, E., Berkowitz, B., 2023. The role of anomalous transport in long-term, stream water chemistry variability. Geophys. Res. Lett. 50, 1–8.

Dewar, R., 2003. Information theory explanation of the fluctuation theorem, maximum entropy production and self-organized criticality in non-equilibrium stationary states. J. Phys. A Math. Gen. 36, 631–641.

Dinelli, E., Cortecci, G., Luchini, F., Zantedeschi, E., 2005. Sources of major and trace elements in the stream sediments of the Arno river catchment (northern Tuscany, Italy). Geochem. J. 39, 531–545.

Egozcue, J.J., Pawlowsky-Glahn, V., Mateu-Figueras, G., Barceló-Vidal, C., 2003. Isometric Logratio transformations for compositional data analysis. Math. Geol. 35, 279–300.

Elter, P., Giglia, G., Tongiorgi, M., Trevisan, L., 1975. Tensional and compressional areas in the recent (Tortonian to present) evolution of the Northern Apennines. Boll. Geofis. Teor. Appl. 17, 3–19.

Gabaix, X., 2016. Power laws in economics: an introduction. J. Econ. Perspect. 30, 185–206.

Gibrat, R., 1930. Une loi des réparations économiques: l'effet proportionnel. Bull. Stat. Gén. Fr. 19, 469.

Gozzi, C., Buccianti, A., 2022. Assessing indices tracking changes in river geochemistry and implications for monitoring. Nat. Resour. Res. 31, 1061–1079.

Gozzi, C., Sauro Graziano, R., Frondini, F., Buccianti, A., 2018. Innovative monitoring tools for the complex spatial dynamics of river chemistry: case study for the alpine region. Environ. Earth Sci. 77, 579.

Gozzi, C., Sauro Graziano, R., Buccianti, A., 2020. Part–whole relations: new insights about the dynamics of complex geochemical riverine systems. Minerals 10 (6), 501.

Hack, J., 1957. Studies of Longitudinal Stream Profiles in Virginia and Maryland. Professional Paper. U.S. Geological Survey.

Kapteyn, J., 1903. Skew Frequency Curves in Biology and Statistics. Astronomical Laboratory Groningen.

Kirchner, J.W., Neal, C., 2013. Universal fractal scaling in stream chemistry and its implications for solute transport and water quality trend detection. Proc. Natl. Acad. Sci. 110, 12213–12218.

Kleidon, A., 2012. How does the Earth system generate andmaintain thermodynamic disequilibrium andwhat does it imply for the future of the planet? Phil. Trans. R. Soc. A 370, 1012–1040.

Kleidon, A., 2016. Thermodynamic Foundations of the Earth System. Cambridge University Press, Cambridge.

Kleidon, A., 2023. Working at the limit: a review of thermodynamics and optimality of the Earth system. Earth Syst. Dynam. 14, 861–896.

Limpert, E., Stahel, W.A., Abbt, M., 2001. Log-normal Distributions across the Sciences: Keys and Clues: on the charms of statistics, and how mechanical models resembling gambling machines offer a link to a handy way to characterize log-normal distributions, which can provide deeper insight into variability and probability—normal or log-normal: that is the question. BioScience 51, 341–352.

Lovejoy, S., 1982. Area-perimeter relation for rain and cloud areas. Science 216, 185–187. https://doi.org/10.1126/science.216.4542.185.

Malamud, B.D., Morein, G., Turcotte, D.L., 1998. Forest fires: an example of self-organized critical behavior. Science 281, 1840–1842. https://doi.org/10.1126/science.281.5384.1840.

Mandelbrot, B., 2003. Multifractal power law distributions: negative and critical dimensions and other "anomalies", explained by a simple example. J. Stat. Phys. 110, 739–774.

Mitzenmacher, M., 2004. A brief history of generative models for power law and lognormal distributions. Internet Math. 1, 226–251.
Moretti, S., 1994. The Northern Apennines. In: Proceeding 76th Summer Meeting of the Italian Geological Society, pp. 739–956.
Newman, M.E.J., 2005. Power laws, Pareto distributions and Zipf's law. Contemp. Phys. 46, 323–351.
Nisi, B., 2005a. Geochimica ed isotopi ambientali nelle acque di scorrimento superficiale della Valle dell'Arno: inquinamento antropico e naturale, vol. 79. APAT (Servizio Geologico d'Italia).
Nisi, B., 2005b. Geochimica ed isotopi ambientali nelle acque di scorrimento superficiale della Valle dell'Arno: inquinamento antropico e naturale. Ph.D. thesis.. University of Florence.
Nisi, B., Buccianti, A., Vaselli, O., Perini, G., Tassi, F., Minissale, A., Montegrossi, G., 2008. Hydrogeochemistry and strontium isotopes in the Arno River Basin (Tuscany, Italy): constraints on natural controls by statistical modeling. J. Hydrol. 360, 166–183.
Ott, W.R., 1990. A physical explanation of the lognormality of pollutant concentrations. J. Air Waste Manage. Assoc. 40, 1378–1383.
Perri, S., Porporato, A., 2022. Environmental concentrations as ratios of random variables. Environ. Res. Lett. 17, 024011 https://doi.org/10.1088/1748-9326/ac4a9f.
Porporato, A., Yin, J., 2022. Ecohydrology: Dynamics of Life and Water in the Critical Zone. Cambridge University Press.
Rinaldo, A., Rodriguez-Iturbe, I., Rigon, R., Bras, R.L., Ijjasz-Vasquez, E., Marani, A., 1992. Minimum energy and fractal structures of drainage networks. Water Resour. Res. 28, 2183–2195.
Rodríguez-Iturbe, I., Rinaldo, A., 2001. Fractal River Basins: Chance and Self-organization. Cambridge University Press.
van Rooij, M., Nash, B., Rajaraman, S., Holden, J., 2013. A fractal approach to dynamic inference and distribution analysis. Front. Physiol. 4, 1.
Seely, A.J.E., Macklem, P., 2012. Fractal variability: an emergent property of complex dissipative systems. Chaos 22, 013108.
Seely, A.J.E., Newman, K.D., Herry, C.L., 2014. Fractal structure and entropy production within the central nervous system. Entropy 16, 4497–4520.
Sornette, D., 2006. Critical Phenomena in Natural Sciences. Chaos, Fractals, Selforganization and Disorder: Concepts and Tools, vol. 2. Springer-Verlag, Berlin Heidelberg.
Vistelius, A.B., 1960. The skew frequency distributions and the fundamental law of the geochemical processes. J. Geol. 68, 1–22.